*Article*

# Analytical Investigation of Magnetic Scalar Potentials Oscillation in Spoke PM Flux Modulation Machines

Lutf Ur Rahman [ID], Abdur Rehman [ID] and Byungtaek Kim *[ID]

Electrical Engineering Department, Kunsan National University, Gunsan-si 573-701, Republic of Korea; lutfurrahman65@yahoo.com (L.U.R.); sengr.abdurrehman@gmail.com (A.R.)
* Correspondence: btkim@kunsan.ac.kr

**Abstract:** In this paper, the oscillation phenomena of the scalar magnetic potential of iron pieces of spoke permanent magnet (PM) machines are analyzed and the effects of the oscillation on the air gap flux and back electro-motive force (EMF) are deeply investigated, especially for flux modulation machines such as vernier and flux switching PM (FSPM) machines. To these ends, the formula of the scalar magnetic potential is derived for a generalized spoke PM structure. It reveals that the oscillation phenomena depend on the slot/pole combination, consequently resulting in different behavior according to the machine types such as vernier and FSPM machines. Next, each core's potential given as a discrete function is developed into a continuous function of an air gap magneto-motive force (MMF) rotating and oscillating through Fourier series expansion. Making use of the developed MMF and the specific permeance of air gap, the equations of air gap flux density and back EMF are derived, which enable accurately estimating the suppression of the modulation flux and the back EMF due to the potential oscillation for different types of spoke PM machines. For validation, various magnetic characteristics are quantitatively examined for different type of spoke PM structures, including PM vernier and FSPM machines, and verified by comparing with FEM simulation results.

**Keywords:** magneto-motive force; modulation flux; scalar magnetic potential; potential oscillation; spoke PM machines

## 1. Introduction

Flux modulation machines (FMMs), due to their higher torque density, are receiving considerable research attention [1–6]. FMMs, due to their higher torque densities, are promising for direct drive applications such as wind turbines [5,7]. FMMs operates on the principle of the magnetic gearing effect, where the gear ratio defines the degree of the magnetic gearing effect [7].

The FMM family, with various topologies, can be classified with PM position and the general surface PM topology; the consequent pole is famous for its magnet saving capability [8], while the spoke PM structure has the advantage of the flux focusing effect, due to which spoke-type topology is often discussed for conventional PM machines [9,10]. The representative FMM spoke types are the spoke PM vernier machine [10] and the flux switching PM (FSPM) machine [11,12]. However, FSPM has the PMs between the stator core pieces in the form of spoke-arrays. In contrast, the PMV machines has the PM on the rotor side.

The slot harmonics of air gap permeance which cause the magnetic gearing effect significantly depend on the effective air gap length [13]. In this respect, a spoke PM vernier machine with an inherently short air gap was tried, and for the first time a phenomenon named as magnetic potential oscillation was found, due to which the modulation flux is rather greatly reduced. This phenomenon of magnetic potential oscillation is actually due to the separation of rotor core pieces, and the previous authors have explained the

leading cause with the harmonic permeance of air gaps that vary with rotor position. Thus, a dual air gap spoke PM structure was recommended to overcome the problem of harmonic permeance variation and, consequently, the magnetic potential oscillation [14]. Later, the phenomenon of magnetic potential oscillation was re-experienced in [15], and a new name, 'flux-barrier effect,' was given to the same phenomenon based on numerical analysis. It was shown that the modulation flux is suppressed by the additional reluctance introduced by an oppositely polarized magnet which acts as a flux barrier in spoke-type FMMs, especially with higher gear ratios. However, for FSPM machines, despite having a spoke structure the same as a vernier machine, it was confirmed through numerical analysis that the reduction of modulation effects severely occurs exceptionally only in a specific gear ratio [15,16]. Unfortunately, in the previous works so far, due to lack of a well-defined analytical approach, it was not possible to analytically explain the development of potential oscillation and, thus, the problem was analyzed based only on the numerical analysis, which greatly limits deep insights into the problem. Moreover, due to the paradoxical nature of magnetic potential oscillation, it was not unified for the class of spoke PM machines. In view of all of these concerns, a generalized analytical model is necessary.

This study presents a generic analytical approach to the phenomena of potential oscillations by improving previous work that was insufficient for predicting the phenomena precisely [14]. In particular, the derived analytical expressions are applicable to any spoke PM machine, although the focus of this study is on FMMs. To this end, first, a general spoke structure is considered and the equation of the magnetic potential of iron pieces is derived from an appropriate hypothesis. The derived equation reveals that the potential oscillation phenomena of iron pieces significantly depend on the slot pole combination. It indicates that the effects of a potential oscillation problem vary with the type of machines, as the criteria for slot-pole selection is different for machine topologies. Next, to obtain the air gap flux density and the back EMF expressions, the potentials of core pieces given as discrete function are developed into a continuous function through Fourier series expansion. The derived expressions are not only helpful to clearly understand the nature of potentials oscillation but also make it possible to quantitatively analyze its effects on the performance of any given spoke PM machine regardless of the slot pole combination. Finally, for validation, magnetic characteristics of various spoke PM prototypes are analyzed analytically and compared with the results obtained by FEM.

## 2. Characteristic Equations Considering Magnetic Potential Oscillation

### 2.1. Generalized Equivalent Circuit Model of a Spoke-Array PM Machine

Figure 1 shows three representative spoke-array PM machines, and each has a different operating principle, specific criteria for the selection of the slot-pole depending on winding configurations. In this study, to obtain a universal expression for potential of any spoke-arrayed core pieces, a generalized model is assumed consisting of an upper core with $Z_U$ slots and a lower core with $Z_L$ iron pieces and spoke-arrayed PMs, as shown in Figure 2a, where $\Omega_k$ is the scalar magnetic potential, $\Phi_k$ is the air gap flux, $\Phi_{m.k}$ is the flux of PM and $\Phi_{leak}$ is leakage flux. Compared with three in Figure 1, the upper core of Figure 2a acts as the stators of conventional PM and vernier machines and as the rotor of FSPM machine.
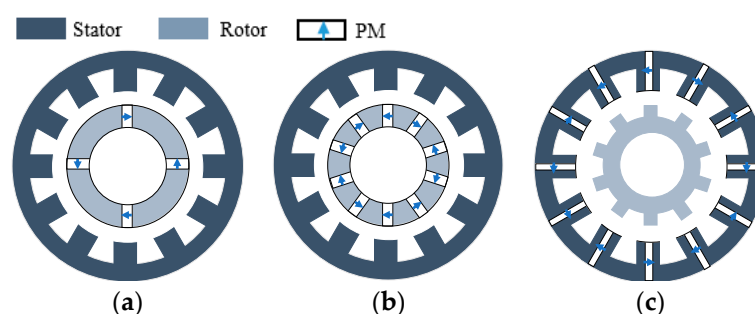


**Figure 1.** Various PM motors with spoke structure. (**a**) Conventional, (**b**) Vernier, (**c**) Flux switching.

(**a**) Generalized model
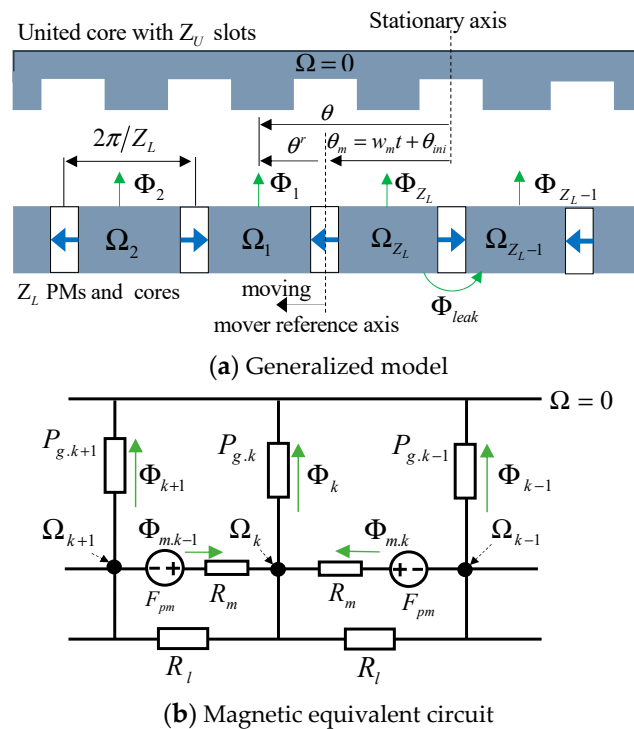


(**b**) Magnetic equivalent circuit

**Figure 2.** Generalized model of PM motors with spoke structure.

The magnetic equivalent circuit of the model of Figure 2a is constructed as Figure 2b where $P_{g.k}$ is the lumped permeance of air gap connected with the $k$th core piece between PMs with MMF $F_{pm}$ and the magnetic reluctance $R_m$, and the reluctance $R_l$ is for the leakage. In particular, $P_{g.k}$ is calculated using the specific permeance as follows.

For ease, the center of the upper slot is set as stationary axis, as shown in Figure 2a. Assuming the lower moves, whose air gap position is $\theta_m$, the upper and the lower sided permeance functions $\Lambda_U$ and $\Lambda_L$ are given respectively as

$$\Lambda_U \approx \lambda_{U0} - \lambda_{U1} \cos Z_U \theta \tag{1}$$

$$\Lambda_L \approx \lambda_{L0} - \lambda_{L1} \cos Z_L (\theta - \theta_m) \tag{2}$$

where $\lambda$ in (1) and (2) are determined by air gap geometries [17]. The net air gap permeance is approximated as

$$\Lambda_g(\theta - \theta_m) \approx \frac{g}{\mu_0} \Lambda_U(\theta) \Lambda_L(\theta, \theta_m) \approx \lambda_{av} - \lambda_{10} \cos Z_U \theta \tag{3}$$

where $g$ is the air gap length, $\lambda_{av} = \frac{g}{\mu_0} \lambda_{U0} \lambda_{L0}$, $\lambda_{10} = \frac{g}{\mu_0} \lambda_{U1} \lambda_{L0}$. With the core stack length $l_{stk}$, and the air gap radius $r_g$, the $k$th lumped permeance $P_{g.k}$ of Figure 2b is obtained as (4) where $\theta_k$ is $\theta_m + \frac{2\pi}{Z_L}(k-1)$.

$$P_{g.k} = r_g l_{stk} \int_{\theta_k}^{\theta_{k+1}} \Lambda_g(\theta, \theta_m) d\theta \tag{4}$$

Letting $\theta^r$ as the angle in mover reference, as shown in Figure 2a, $\theta_k$ can be expressed as $\theta_k^r + \theta_m$. Solving (4) with (1)~(3), one can get (5)

$$P_{g.k}(\theta_m) = P_{av} - P_\Delta \cos(Z_U \theta_k^r + Z_U \theta_m + \gamma_z \pi) \tag{5}$$

where $P_{av} = r_g l_{stk} \lambda_{av} \frac{2\pi}{Z_L}$, $P_\Delta = P_1 \sin \gamma_z \pi$, $P_1 = r_g l_{stk} \lambda_{10} \frac{2}{Z_U}$, and $\gamma_z = \frac{Z_U}{Z_L}$. It should be noticed that $P_{g.k}$ oscillates with the mover position $\theta_m$ due to the 2nd term in (5).

### 2.2. Analytical Expressions of Scalar Magnetic Potential

From Figure 2b, the following relations for flux $\Phi$, (6), and (7) can be obtained for the $k$th core piece.

$$\Omega_k P_{g.k} = \Phi_{m.k-1} + \Phi_{m.k} \tag{6}$$

$$\left.\begin{array}{c} \Phi_{m.k} = \left(\Omega_{k+1} + F_{pm'} - \Omega_k\right) R_{m'} \\ \Phi_{m.k-1} = \left(\Omega_{k-1} + F_{pm'} - \Omega_k\right) R_{m'} \end{array}\right\} \tag{7}$$

where $F_{pm'} = F_{pm} R_l / (R_m + R_l)$ and $R_{m'} = R_m || R_l$. Substituting (7) into (6) yields the following.

$$(-1)^{k-1} 2 F_{pm'} = \left(2 + P_{g.k} R_{m'}\right) \Omega_k - \left(\Omega_{k-1} + \Omega_{k+1}\right) \tag{8}$$

If without $P_\Delta$ in (5), $P_{g.k}$ is constant with respect to mover position and the core pieces have the same magnitude of magnetic scalar potentials but alternating signs. Then, the potential $\Omega_k$ given as the form of $(-1)^{k-1}\Omega_{av}$ is easily solved from (8). However, $P_{g.k}$ with $P_\Delta$ varies with mover position; causing $\Omega_k$ also does, and it is tricky to directly achieve the analytical solution of $\Omega_k$ using (8). Thus, in this study, a trial function is assumed to get the proper expression of $\Omega_k$.

Under the hypothesis that the harmonics of $Z_U$ and $Z_L/2$ of $P_{g.k}$ produces the modulation harmonic of $|Z_U - Z_L/2|$ in $\Omega_k$, the function (9) neglecting high order harmonics is tried, where $Z_L/2$ is replaced with the PM pole pairs $Z^{PM}$ and $(-1)^{k-1}$ is replaced with $\cos(Z^{PM}\theta_k^r)$ because of $\theta_k^r = \frac{\pi}{Z^{PM}}(k-1)$. The magnitudes $\Omega_{av}$ and $\Omega_{\Delta 1}$ need to be determined to satisfy (8), and using (9), with consideration of the PM direction, $\Omega_{k-1} + \Omega_{k+1}$ in (8) can be calculated as (10).

$$\Omega_k = \cos Z^{PM}\theta_k^r \cdot \Omega_{av} + \Omega_{\Delta 1} \cos\left(\left(Z_U - Z^{PM}\right)\theta_k^r + Z_U\theta_m + \gamma_z\pi\right) \tag{9}$$

$$\Omega_{k-1} + \Omega_{k+1} = -2\Omega_k + 4\Omega_{\Delta 1} \sin^2 \gamma_z\pi \cos\left(\left(Z_U - Z^{PM}\right)\theta_k^r + Z_U\theta_m + \gamma_z\pi\right) \tag{10}$$

Solving (8) for $\Omega_k$ using (10), one gets

$$\begin{aligned} \Omega_k \quad &= \frac{2}{4 + R_{m'}P_{av}} \cdot \frac{1}{1 - K_p \cos(Z_U\theta_k^r + \gamma_z\pi)} \Big\{ \cos Z^{PM}\theta_k^r \cdot F_{pm'} \\ &+ 2\Omega_{\Delta 1} \sin^2 \gamma_z\pi \cos\left(\left(Z_U - Z^{PM}\right)\theta_k^r + Z_U\theta_m + \gamma_z\pi\right) \Big\} \end{aligned} \tag{11}$$

where the coefficient in the second multiplication term,

$$K_p = \frac{R_{m'}P_\Delta}{4 + R_{m'}P_{av}} = \frac{R_{m'}P_1}{4 + R_{m'}P_{av}} \sin \gamma_z\pi \tag{12}$$

To determine $\Omega_{av}$ and $\Omega_{\Delta 1}$ by comparing (11) and (9), the 2nd factor of (11) is changed into Fourier series as

$$\left\{1 - K_p \cos(Z_U\theta_k^r + \gamma_z\pi)\right\}^{-1} = k_0 + \sum_{i=1} k_i \cos i(Z_U\theta_k^r + \gamma_z\pi) \tag{13}$$

where $k_0 = 1/\sqrt{1 - K_p^2}$ and $k_1 = 2(k_0 - 1)/K_p$.

Substituting (13) into (11), one gets

$$\begin{aligned} \Omega_k = \left(\cos Z^{PM}\theta_k^r\right) \frac{2k_0 F_{pm'}}{(4 + R_{m'}P_{av})} + \frac{4\Omega_{\Delta 1}\sin^2\gamma_z\pi + 2k_1 F_{pm'}}{4 + R_{m'}P_{av}} \times \\ \cos\left(\left(Z_U - Z^{PM}\right)\theta_k^r + Z_U\theta_m + \gamma_z\pi\right) + \text{higher order harmonics} \end{aligned} \tag{14}$$

$\Omega_k$ of (14) contains additional higher harmonics neglected in (9), which confirms that $\Omega_k$ of (9) is an approximate solution as assumed. Finally, from (14) and (9), $\Omega_{av}$ and $\Omega_{\Delta 1}$ are given as

$$\Omega_{av} = \frac{2F_{pm'}}{(4 + R_{m'}P_{av})} \cdot \frac{1}{\sqrt{1 - K_p^2}} \tag{15}$$

$$\Omega_{\Delta 1} = 2\Omega_{av} \cdot \frac{1 - \sqrt{1 - K_p^2}}{K_p^2} \cdot \left(1 - \frac{4\sin^2 \gamma_z \pi}{(4 + R_{m'}P_{av})\sqrt{1 - K_p^2}}\right)^{-1} \tag{16}$$

Now, the potential $\Omega_k$ of (9) is apparently defined with (15) and (16), which indicates both the fixed potential value $\Omega_{av}$ and the oscillation amplitude $\Omega_{\Delta 1}$ are affected by $\gamma_z$ because $K_p$ of (12) is also dependent on $\gamma_z$. In particular, $K_p$ must be much smaller than unity because $P_{av}$ is much larger than $P_\Delta$ in (12). Hence, it can be said that $\gamma_z$ ($Z_U/Z_L$); that is, the combination of slots and PM poles has much larger effects on $\Omega_{\Delta 1}$ than $\Omega_{av}$.

*2.3. Air Gap Magneto-Motive Force*

It is necessary to multiply the air gap MMF with specific air gap permeance in order to get the air gap flux density and the back EMF. The air gap MMF is the difference of the magnetic potentials of the upper and the lower cores, and the potential of the upper core is zero (see Figure 2), so the obtained potential of (9) can be directly used for the air gap MMF $F_g$ given as

$$F_g(\theta^r) = (-1)^{k-1}\Omega_{av} + \Omega_{\Delta 1}\cos\left((Z_U - Z^{PM})\theta_k^r + Z_U\theta_m + \gamma_z\pi\right) \\ \text{for } \theta_k^r < \theta^r < \theta_k^r, k = 1, 2 \ldots, Z_L \tag{17}$$

which is a piecewise function expressed in mover reference frame using the angular position $\theta^r$. However, $F_g$ of (17) is in a very inconvenient form to multiply with the permeance of (3). Therefore, it is helpful to change it into a continuous series function, especially in stationary reference frame as (3). Let the 1st and the 2nd term of (17) be $F_g^{av}$ and $F_g^\Delta$, respectively. Since $F_g^{av}$ is a square wave with the period of $2\pi/(Z_L/2)$ in mover reference frame, it can be easily changed into Fourier series form and into the stationary reference frame using the relation $\theta^r = \theta - \theta_m$ as follows

$$\begin{aligned} F_g^{av}(\theta^r) &= (-1)^{k-1}\Omega_{av} \text{ for } \theta_k^r \leq \theta^r < \theta_{k+1}^r \\ &= \frac{4}{\pi}\Omega_{av} \sum_{n=odd} \frac{1}{n}\sin nZ^{PM}(\theta - \theta_m) \end{aligned} \tag{18}$$

Similarly, using the Fourier series $F_g^\Delta$, can be represented as (19), the detailed derivation procedure of $F_g^\Delta$, is in Appendix A.

$$F_g^\Delta = \frac{\Omega_{\Delta 1}}{\pi}\cos \gamma_z \pi \sum_{n=odd} \pm \frac{2\sin\left((Z_U \pm nZ^{PM})\theta \mp nZ^{PM}\theta_m\right)}{n \pm 2\gamma_z} \tag{19}$$

Now, letting the modulation pole pairs $Z_{n\pm}^{mod}$ as

$$Z_{n\pm}^{mod} = Z_U \pm nZ^{PM} \tag{20}$$

using (18) and (19), the air gap MMF $F_g$ is finally obtained as

$$F_g = \sum_{n=odd} \left\{ \begin{array}{l} F_n^{av}\sin nZ^{PM}(\theta - \theta_m) - F_{n-}^\Delta \sin\left(Z_{n-}^{mod}\theta + nZ^{PM}\theta_m\right) \\ +F_{n+}^\Delta \sin\left(Z_{n+}^{mod}\theta - nZ^{PM}\theta_m\right) \end{array} \right\} \tag{21}$$

where $F_n^{av} = \frac{4\Omega_{av}}{\pi n}$, $F_{n-}^\Delta = \frac{\Omega_{\Delta 1}}{\pi}\frac{\cos \gamma_z \pi}{0.5n - \gamma_z}$, and $F_{n+}^\Delta = \frac{\Omega_{\Delta 1}}{\pi}\frac{\cos \gamma_z \pi}{0.5n + \gamma_z}$.

The 1st term of (21) is the general MMF wave of every PM machine with $Z^{PM}(=Z_L/2)$ pole pairs including the surface PM vernier. However, the 2nd and the 3rd term are unique waves that appeared in a spoke-array PM structured machine due to the oscillation of the scalar magnetic potential of each core. Thus, there is inevitable influences on the air gap flux density and back EMF predominantly due to the MMF waves.

*2.4. Air Gap Flux Density and Back EMF*

Multiplying the air gap permeance of (3) and the MMF of (21) the air gap flux density is approximated as

$$B_g^{low}(\theta) \approx \sum_{n=odd} \left\{ \begin{array}{l} \left( \lambda_{av} F_n^{av} - \lambda_{10} \frac{F_{n-}^{\Delta} - F_{n+}^{\Delta}}{2} \right) \sin nZ^{PM}(\theta - \theta_m) \\ \pm \left( \frac{\lambda_{10} F_n^{av}}{2} - \lambda_{av} F_{n\mp}^{\Delta} \right) \sin \left( Z_{n\mp}^{mod} \theta \pm nZ^{PM} \theta_m \right) \end{array} \right\} \tag{22}$$

The flux density $B_g$ of (22) has been derived with the lower body as a mover in Figure 2a, so it can be used for a vernier and a conventional machine since their windings are installed in the upper body. However, the frequency of the back EMF in the stator winding by the flux of (22) is determined by the coefficient of $\theta_m$. Since vernier and conventional PM machines use the fundamental PM flux in common, the coefficient of $\theta_m$ should be the same as $Z^{PM}$. In addition, one in the 2nd term in (22) induces negligible voltage due to its low speed of $Z^{PM}/Z_{1+}^{mod}$. Consequently, the working flux for the conventional and vernier machines are as follows.

$$B_{work}^{low}(\theta) \approx \sum_{n=odd} \left\{ \begin{array}{l} \left( \lambda_{av} F_1^{av} - \lambda_{10} \frac{F_{1-}^{\Delta} - F_{1+}^{\Delta}}{2} \right) \sin Z^{PM}(\theta - \theta_m) \\ + \left( \frac{\lambda_{10} F_1^{av}}{2} - \lambda_{av} F_{1-}^{\Delta} \right) \sin \left( Z_{1-}^{mod} \theta + Z^{PM} \theta_m \right) \end{array} \right\} \tag{23}$$

where the 1st term is commonly called the main flux and the 2nd is the modulation flux. Their back EMF is the time derivative of the flux linkage due to (23) so it has a relation given as

$$\begin{aligned} E_{ph}^{low} &\propto \left\{ k_{w1}^{main} \left( \lambda_{av} F_1^{av} - \lambda_{10} \frac{F_{1-}^{\Delta}}{2} \right) + \left( \frac{\lambda_{10} F_1^{av}}{2} - \lambda_{av} F_{1-}^{\Delta} \right) G_1^{low} \right\} \\ &= K_c \left\{ k_{w1}^{main} \left( \lambda_{av} F_1^{av} - \lambda_{10} \frac{F_{1-}^{\Delta}}{2} \right) + \left( \frac{\lambda_{10} F_1^{av}}{2} - \lambda_{av} F_{1-}^{\Delta} \right) G_1^{low} \right\} \end{aligned} \tag{24}$$

where $K_c$ is the coefficient related to the number of turn ($N_{ph}$), machine geometry that is radius of airgap ($r_g$) and stack length ($l_{stk}$), and rotational speed ($\omega_m$). $G_1^{low}$ is the gear ratio given as $Z^{PM}/Z_{1-}^{mod}$ for the conventional and vernier PM machines. The coefficients $k_{w1}^{main}$ and $k_{w1}^{mod}$ are the winding factors for two fluxes in (24) and depend on the coil span of winding, so the span needs to be properly chosen. In case of 3-phase concentrated windings, the winding factor for each harmonic can be obtained by $k_{wn}^{main} = \left| \sin \left( nZ^{PM} \theta_{span}/2 \right) \right|$ where $\theta_{span}$ is the mechanical angular span of each coil.

On the other hand, in the case of an FSPM, whose PMs and windings are installed in a stator, (22) should be modified considering the motion of the upper body instead of the lower, which is achieved by changing $\theta$ with $\theta + \theta_m$ given as,

$$B_g^{up}(\theta) \approx \sum_{n=odd} \left\{ \begin{array}{l} \left( \lambda_{av} F_n^{av} - \lambda_{10} \frac{F_{n-}^{\Delta} - F_{n+}^{\Delta}}{2} \right) \sin nZ^{PM} \theta \\ \pm \left( \frac{\lambda_{10} F_n^{av}}{2} - \lambda_{av} F_{n\mp}^{\Delta} \right) \sin \left( Z_{n\mp}^{mod} \theta + Z_U \theta_m \right) \end{array} \right\} \tag{25}$$

It is evident that in the 1st term of (25), the main flux remains static, and thus only the modulation fluxes are able to produce the back EMF. In particular, it should be noted that

the frequencies of back EMF due to the modulation fluxes are all the same, $Z_U$. As results the working flux and the back EMF for the FSPM are given by

$$B_{work}^{up}(\theta) \approx \sum_{n=odd} \left( \frac{\lambda_{10} F_n^{av}}{2} - \lambda_{av} F_{n-}^{\Delta} \right) \sin \left( Z_{n-}^{mod} \theta + Z_U \theta_m \right) \tag{26}$$

$$
\begin{aligned}
E_{work}^{up} &\propto \sum_{n=odd} k_{wn}^{mod} \left( \frac{\lambda_{10} F_n^{av}}{2} - \lambda_{av} F_{n-}^{\Delta} \right) G_n^{up} \\
&= K_c \sum_{n=odd} k_{wn}^{mod} \left( \frac{\lambda_{10} F_n^{av}}{2} - \lambda_{av} F_{n-}^{\Delta} \right) G_n^{up}
\end{aligned}
\tag{27}
$$

where $G_n^{up}$ is the gear ratio given as $Z_U / Z_{n-}^{mod}$. Comparing the back EMF expressions of (24) and (27), the FSPM machine does not utilize the main flux but does various harmonic modulation fluxes to get the back EMF while the conventional and the vernier machines make use of just the fundamental fluxes of the main and the modulation fluxes.

### 2.5. Suppression Characteristics of Modulation Flux Due to Magnetic Potential's Oscillation

From (22) to (27), it is also evident that the term $\lambda_{av} F_{n-}^{\Delta}$ in the parenthesis, arisen due to the potentials oscillation in spoke array PM structure, suppresses the modulation flux $(\lambda_{10} F_n^{av})/2$ and, thus, results in the reduction of back EMF. In particular, this unique phenomenon occurs differently for the types of the machines because $F_{n-}^{\Delta}$ is dependent on $\gamma_z$ (slot-pole combination). To quantitatively evaluate the suppression of the modulation flux when the coefficient $\alpha_n^{BL}$ is defined as

$$\alpha_n^{BL} = 2 \frac{\lambda_{av}}{\lambda_{10}} \frac{F_{n-}^{\Delta}}{F_n^{av}} \tag{28}$$

and then the back EMF due to the modulation flux in (24) and (27) can be given as (29). Thus, $\alpha_n^{BL}$ indicates the reduction rate of the modulation flux with the n$^{th}$ harmonic order

$$E_{mod}^{up,low} \propto \frac{\lambda_{10}}{2} \sum_{n=odd} k_{w.n} F_n^{av} \left( 1 - \alpha_n^{BL} \right) G_n^{up,low} \tag{29}$$

In order to quantitatively calculate $\alpha_n^{BL}$ with variation of the ratio $\gamma_z$, the realistic geometries of spoke PM structures are assumed for which the PM thickness $w_m$ is $1/5$ of the pole arc length and the PM height $h_m$ is the pole arc length. Under these assumptions the PM reluctance, $R_m$ becomes $\frac{w_m}{\mu_0 h_m l_{stk}} = \frac{0.2}{\mu_0 l_{stk}}$. In addition, assuming that the ratio $r_g / g$ is 100, one gets $R_m R_{av} = \frac{40\pi}{k_c Z_L}$ and $R_m R_1 = \frac{1}{k_c} \frac{\lambda_{10}}{\lambda_{av}} \frac{40}{Z_L}$ where $k_c$ is Carter's coefficient considering both the upper and the lower slots, and then $K_p$ of (12) becomes

$$K_p = \frac{\lambda_{10}}{\lambda_{av}} \frac{10}{k_c Z_L + 10\pi} \frac{\sin \gamma_z \pi}{\gamma_z} \tag{30}$$

Consequently, the reduction rate $\alpha^{BL}$ is given as (31), which reveals the reduction rate of modulation depends on $Z_L$ as well as $\gamma_z$, that is, $Z_U / Z_L$. For $0 \le \gamma_z \le 2.5$ and various values of $Z_L$, the values of $\alpha_n^{BL}$ are calculated and shown in Figure 3 in which the gear ratios $\left| G_1^{low} \right|$ for a vernier machine and $|G_n^{up}|$ for FSPM are also depicted.

$$\alpha_n^{BL} = \frac{\lambda_{av}}{\lambda_{10}} \frac{1 - \sqrt{1 - K_p^2}}{K_p^2} \left( 1 - \frac{\sin^2 \gamma_z \pi}{\left(1 + \frac{10\pi}{k_c Z_L}\right) \sqrt{1 - K_p^2}} \right)^{-1} \left( \frac{n \cos \gamma_z \pi}{0.5n - \gamma_z} \right) \tag{31}$$

Figure 3 shows that when $\gamma_z$ gets closer to $0.5 \, n$ where $n$ is an odd integer, the ratio $G_n$ for nth harmonic approaches infinity but the reduction rate $\alpha_n^{BL}$ also gets unity (meaning most of the nth modulation flux are lost). Conversely, when $\gamma_z$ is an integer, all $\alpha_n^{BL}$ are zero (no reduction for any modulation flux), but most gear ratios are quite small. To be exact,

as the integer $\gamma_z$ increases, the ratio $G_n^{up}$ gradually increases although its corresponding harmonic MMF $F_n^{av}$ in (26) reduces.
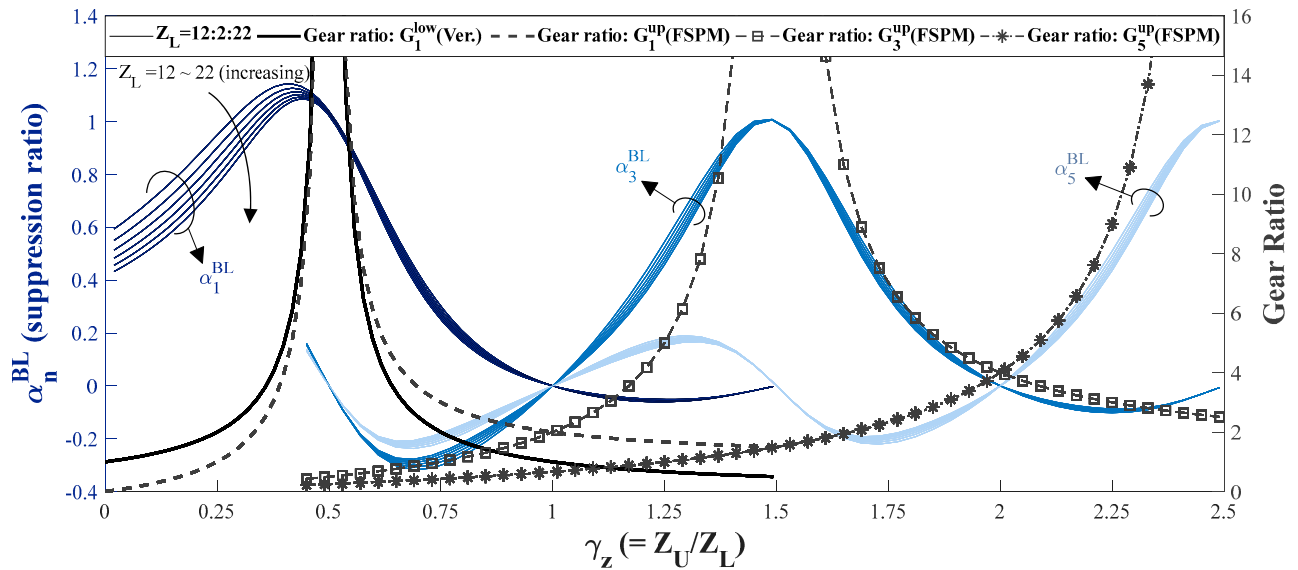


**Figure 3.** Suppression ratio and gear ratio of harmonic modulation fluxes with $\gamma z$ (=$Z_U/Z_L$).

It can be concluded that in the case of a spoke-array PM FMMs, the gear ratio $G_n$ and the reduction rate $\alpha_n^{BL}$ of the $n$th modulation flux tend to be proportional to each other. Therefore, it is difficult to obtain high magnetic gear effects due to the potential oscillation phenomena, and this phenomenon is more severe for the 1st harmonic ($n = 1$).

### 3. Potentials Oscillation Behavior in Various Spoke PM Machines

The three spoke PM machines in Figure 1 have unique operation principles and specific criteria for selection of slot-pole combination. In this section, using the derived Equations (22)–(27), the reduction coefficient $\alpha_n^{BL}$ and the results of Figure 3, the nature of potential oscillations for each spoke PM machine is discussed in which the machine's own criteria of slot-pole combination is separately considered for the integral slot (IS) and fractional slot concentrated (FSC) windings.

### 3.1. Conventional Spoke PM Machine

Conventional PM machines were classically devised to utilize the main flux only, and the modulation flux has a negligible contribution [18], due to the small values of $G_1^{low}$ in (24) regardless the presence of the potential oscillation. Thus, potential oscillations are briefly discussed.

In case of the IS windings, the slot-pole combination is as follows; the PM Pole pairs, $Z^{PM}(=Z_L/2)$ of (23) is same to the winding pole pairs $p_w$. To obtain the pole pairs, the stator slots, $Z_U$ in Figure 2 should 6 $p_w m$ in 3-phase windings where $m$ is a positive integer. Hence, $\gamma_z$ must be an integer, and the modulation fluxes have no suppression as shown in Figure 3.

For FSC winding, available slot-pole combinations are numerous and the concept of winding pole pair becomes unclear, making it difficult to define the combination criteria in a simple manner. Thus, as examples the most popular slots/PMs ratio of 3/4 and 3/2 are examined. From Figure 3, when $\gamma_z$ is 3/4, $G_1^{low}$ is about 2 and $\alpha_1^{BL}$ is about 0.3, resulting in trivial contribution to the back EMF. Also, for $\gamma_z = 3/2$, $G_1^{low}$ is 0.5 negligibly small. In conclusion, the conventional machine is free from potential oscillation issues, but the magnetic gear effect is also small enough to be ignored.

### 3.2. Spoke PM Vernier Machine

The windings of FMMs are configured to use the modulation flux in (23). It leads to the condition for IS winding, $p_w = Z_{1-}^{mod}$ under which $k_{w1} \approx 1$. The condition can be rewritten as (32). Replacing the stator slots $Z_U$ in (32) with $6 p_w m$, the PM poles $Z_L$ can be obtained as $2 p_w (6 m - 1)$. The ratio $\gamma_z (= Z_U / Z_L)$ becomes $3 m / (6 m - 1)$ and the ranges of $\gamma_z$ with a positive integer $m$ can be given by (33)

$$p_w = Z_{1-}^{mod} = Z_U - Z^{PM} \tag{32}$$

$$0.5 < \gamma_z = 3m/(6m - 1) < 0.6 \tag{33}$$

According to Figure 3, the gear ratio, $G_1^{low}$ is 5 at $\gamma_z = 0.6$ (for $m = 1$) and significantly increases as $m$ increases. Therefore, it is beneficial to use larger $m$ for surface PM vernier machines. For the spoke PM structure, however, the corresponding reduction ratio $\alpha_1^{BL}$ is also greater than about 0.75, so the back EMF achieved from the modulation flux is severely reduced, as discussed in [15].

Additionally, from (24), it is worth noting that both main and modulation flux simultaneously contribute to the back EMF. The PM pole pairs $Z_L / 2$ is $p_w (6 m - 1)$, an odd multiple of the winding pole pairs $p_w$, yielding $k_{w1}^{main}$ of (24) close to 1. As the permeance $\lambda_{av}$ is quite large compared to the harmonic one $\lambda_{10}$, the PM vernier machine additionally receives back EMF from the main flux, this is why the back EMF of a surface PM vernier machine is superior to the conventional machine's [19].

The FSC winding can be configured to use the 1st harmonic modulation flux. In the conventional fluxes discussed previously, the slots-PMs ratio of 3/2 (or 3/4) implies that 2 (or 4) pole length of the main flux is divided by 3 stator slots. Similarly, in the vernier machine with $Z_U$ stator slots and $Z_L$ rotor PMs, the stator slots in the 2 (or 4) pole length of the modulation flux with $Z_{1-}^{mod}$ pole-pairs is divided into thirds. The condition for these is given as $(Z_U / m) / (2 Z_{1-}^{mod}) = \alpha$ in which $\alpha$ is 3/4 or 3/2 and replacing $Z_{1-}^{mod}$ with $Z_U - 0.5 Z_L$, one gets

$$\gamma_z (= Z_U / Z_L) = \alpha m / (2 \alpha m - 1) \tag{34}$$

It is interesting that for $m = 1$, $\gamma_z$ becomes 3/2 and 3/4 when $\alpha = 3/4$ and 3/2, respectively, which are the same $\gamma_z$ of the conventional PM machine. In other words, two vernier machines for $m = 1$ belong to the conventional PM machines. In addition, for $m = 2$ and $\alpha = 3/4$, $\gamma_z$ also becomes 3/4 of conventional machines. Thus, they have very small gear ratio $G_1^{low}$ less than 2 or useless infinity. For $m \geq 2$ except 3 cases above, the range of $\gamma_z$ is given as $0.5 < \gamma_z < 0.6$ which are same to that for the IS windings (33) and, thus, the same phenomena happen to the machine.

### 3.3. Flux Switching PM Machine

Different from a PM vernier, an FSPM has both the excitation sources on the stator represented by the lower body of Figure 2a. Hence, $Z_U$ and $Z_L$ represent the number of rotor teeth and PM poles, respectively, in FSPM structure, and only the modulation fluxes are responsible for back EMF production as discussed. Recalling that the spoke PM vernier machine hardly uses the gear effects due to potential oscillations, it seems natural to guess the similar conclusion for FSPM with spoke PMs. But the existing literature on FSPMs have rarely mentioned the problems related with potentials oscillation. Thus, the investigations on potentials oscillation and its effects on the FSPM is worthwhile.

As shown in (26) and (27), the back EMF of FSPM is the sum of each back EMF caused by various harmonic modulated magnetic fluxes excluding the main flux. Therefore, in order to predict the back EMF, for each harmonic component it is necessary to consider the gear ratio $G_n^{up}$, the reduction rate $\alpha_n^{BL}$ and the winding factor $k_{wn}^{mod}$ for a given winding. The relation (20) can be given as $Z_{n-}^{mod} = Z_U - n Z_L / 2$ in which $Z_L$ is the number of stator

slots of FSPM, so $Z_L$ varies depending on the winding configurations and the number of poles of the modulation flux.

First, in the case of an FSPM having integral (*m*) slot distributed winding with the winding pole pairs $p_w = Z_{1-}^{mod}$, the stator slots $Z_L$ is 6 $p_w m$, so the rotor slots $Z_U$ becomes $(3\ m + 1)p_w$ and finally the ratio $\gamma_z$ (=$Z_U/Z_L$) is given as

$$0.5 < \gamma_z \leq 0.66 \tag{35}$$

In the range of (35) in Figure 3, $G_1^{up}$ is larger than 4, and $k_{w1}^{mod}$ for the modulation flux with $Z_{1-}^{mod}$ pole pairs is close to 1. However, the corresponding $\alpha_1^{BL}$ is also quite large as 0.5 or more, reducing the gear effects. In addition, both $G_3^{up}$ and $G_5^{up}$ are less than 1 and their winding factors $k_{w3,5}^{mod}$ become also much smaller since $Z_{n-}^{mod}$ is not the multiples of $Z_{1-}^{mod}$. Therefore, there is little contribution from the harmonic modulation fluxes regardless $\alpha_{3,5}^{BL}$. Consequently, the IS winding is improper for FSPM even if it has a considerable gear ratio for $Z_{1-}^{mod}$.

Second, for the FSC winding, assuming that 2 or 4 poles of the 1st modulation flux wave are equally divided into 3 slots, one gets the relation $\frac{Z_L}{Z_{n-}^{mod}} = \frac{Z_L}{2(Z_U - 0.5Z_L)} = \frac{3}{2}$ or $\frac{3}{4}$ and $\gamma_z$ of $Z_U/Z_L$ is calculated as 5/6 and 7/6 for the ratio of 3/2 and 3/4 respectively.

Examining the gear ratios and reduction ratios, when $\gamma_z = 5/6$, $G_{1,3,5}^{up} = 2.5, 1.25, 0.5$ and $\alpha_{1,3,5}^{BL} = 0.15, -0.23, -0.15$, and when $\gamma_z = 7/6$, $G_{1,3,5}^{up} = 3.5, 1.75, 0.87$ and $\alpha_{1,3,5}^{BL} = -0.07, 0.4, 0.16$. It indicates, for FSC windings, the gear ratios for various harmonic modulation fluxes are neither too large nor too small. In addition, some of the reduction ratios have negative values that increase the modulation fluxes. Considering the coil span $\theta_{span} = 2\pi/Z_L$ for FSC windings, the winding factor $k_{wn}^{mod}$ for all harmonics is equally 0.87 as given by

$$k_{nw}^{mod} = \left| \sin\left(\frac{1}{2} Z_{n-}^{mod} \theta_{span}\right) \right| = |\cos \gamma_z \pi| \approx 0.87 \tag{36}$$

Based on the above, every harmonic modulation flux contributes to back EMF production with almost no reduction, which is why most common FSPMs have FSC despite their non-significant gear ratio $G_1^{up}$.

## 4. Validation with Case Studies

### 4.1. Analysis Models

For validation, four prototype models shown in Figure 4 are designed, the main design parameters are given in Table 1. For each prototype the PM dimensions are selected as per the predefined assumption.
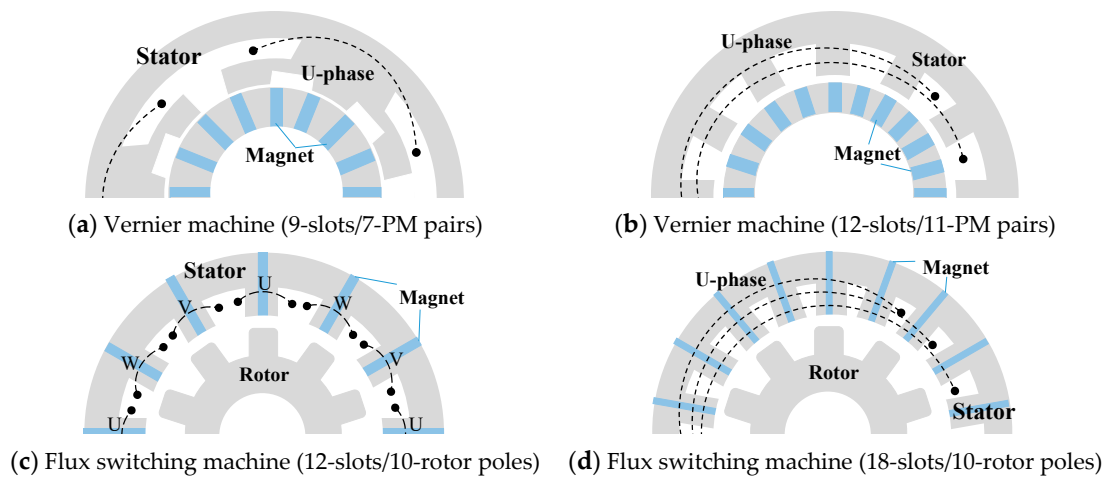


(**a**) Vernier machine (9-slots/7-PM pairs)　　　(**b**) Vernier machine (12-slots/11-PM pairs)

(**c**) Flux switching machine (12-slots/10-rotor poles)　　(**d**) Flux switching machine (18-slots/10-rotor poles)

**Figure 4.** Designed spoke PM machines for analysis.

**Table 1.** Main Design Parameters of the Prototype Models.

| Parameters | Vernier Spoke PM Machine (Figure 4a,b) | | Flux Switching Spoke PM Machine (Figure 4c,d) | |
|---|---|---|---|---|
| Gear ratio | $G_1^{low} = 3.5$ | $G_1^{low} = 11$ | $G_{1,3,5}^{up} = 2.5, 1.25, 0.5$ | $G_{1,3,5}^{up} = 10, 0.58, 0.28$ |
| Winding type | FSC | IS | FSC | IS |
| Air-gap radius | 100 mm | | | |
| Stack length | 50 mm | | | |
| Air-gap length | 1 mm | | | |
| Magnet height | 44.8 mm | 28.5 mm | 52.5 mm | 35 mm |
| Magnet width | 8.9 mm | 5.7 mm | 10.5 mm | 6.9 mm |
| No. of slots, $Z_U$ | 9 | 12 | 10 | 10 |
| PM poles, $Z_L$ | 14 | 22 | 12 | 18 |
| Rotational speed | 600 rpm | | | |
| Turns per Phase | 200 | | | |
| $\gamma_z$ (=$Z_U/Z_L$) | 0.64 | 0.54 | 0.833 | 0.56 |
| Suppression ratio $\alpha_n^{BL}$(%) | $\alpha_1^{BL} = 58\%$ | $\alpha_1^{BL} = 89\%$ | $\alpha_{1,3,5}^{BL} = 15\%, -23\%, -15\%$ | $\alpha_{1,3,5}^{BL} = 84\%, -15\%, -13\%$ |

The conventional spoke PM machine is not chosen for analysis as it has negligible contribution form the modulation flux, so the suppression of modulation flux is irrelevant. However, for spoke PM FMMs, where the modulation flux plays an important role, the modulation flux is expected to be suppressed very differently depending on the gear ratio. To prove this, for each spoke PM vernier machine and FSPM, two models with lower/higher gear ratio are selected, as shown in Figure 4, and their gear ratios, $\gamma_z$ and the suppression ratios $\alpha_n^{BL}$ are given in Table 1 as well as depicted in Figure 5. It can be noticed that models with higher gear ratios have relatively higher $\alpha_n^{BL}$.
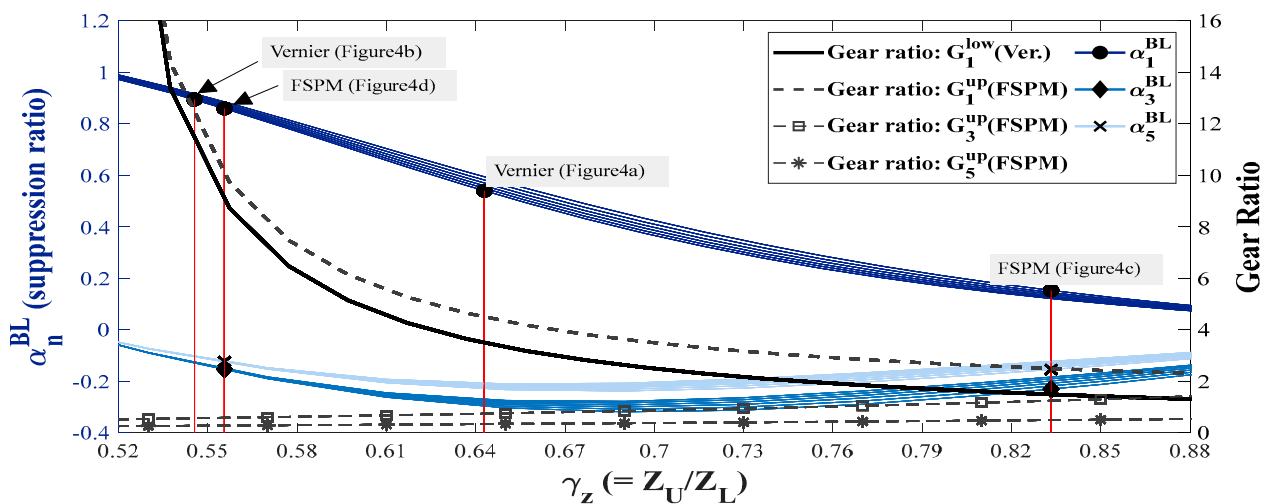


**Figure 5.** Suppression ratio and gear ratio of harmonic modulation fluxes with $\gamma_z$ (=$Z_U/Z_L$) of all analysis models (reproduced from Figure 3).

As far as the winding configuration is concerned, $\gamma_z$ of spoke vernier is irrespective of the winding configuration. But for FSPM, $\gamma_z$ and, hence, $\alpha_n^{BL}$ depend on the winding configuration and usually FSPM with higher gear ratios are feasible with IS winding. Thus, FSPM with lower and higher gear ratio are designed with FSC and IS windings.

### 4.2. Procedure for Verification with FEM

In order to demonstrate the suppression phenomena of the spoke FMMs, both the magnetic characteristics with/without considering the potential oscillations for each prototype are analytically obtained and are compared, including FEM results.

As discussed, the suppression of the modulation flux is fundamentally caused by the potentials oscillation of the iron core pieces and its effect in analytical expressions starts from the existence of $K_p$ in (14) and (15). If $K_p = 0$, the oscillation magnitude $\Omega_{\Delta 1}$ of (16) and $F_{n\pm}^{\Delta}$ in (21) are made to 0, and the effects of potentials oscillation are neglected on the air gap MMF and flux density. With/without $K_p$, for each model, the flux density and the back EMF is obtained and compared with the FEM results. The discussion clearly reveals the effect of potentials oscillation on suppression for each prototype.

#### 4.2.1. Vernier Machine

The two spoke vernier prototypes of Figure 4a,b have $Z^{PM}$ of 7 and 11, $Z_{1-}^{mod}$ of 2 and 1, and gear ratio $G_1^{low}$ of 3.5 and 11, respectively. For both the models, the air gap MMF of (21) has been obtained with/without the potentials oscillation (their waveform is depicted in Appendix B, Figure A1), and their harmonics are illustrated in Figure 6($a_1$,$a_2$). There is a slight increase in $F_1^{av}$ when potential oscillations are considered due to non-zero $K_p$ in (15). It should be noticed that the $Z_{1-}^{mod}$ th oscillating MMF $F_{1-}^{\Delta}$ for both models expected to suppress the modulation flux is considerable, and that of Figure 4b with higher $G_1^{low}$ is larger.
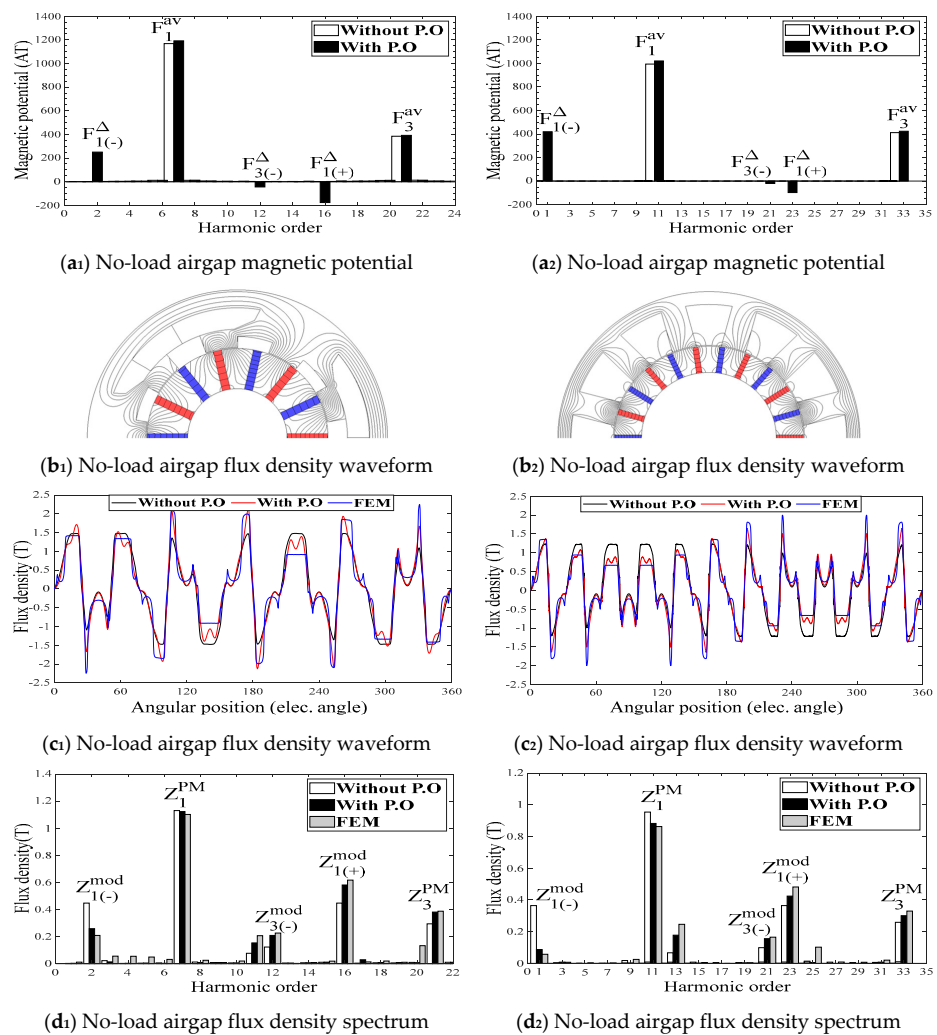


(**a₁**) No-load airgap magnetic potential

(**a₂**) No-load airgap magnetic potential

(**b₁**) No-load airgap flux density waveform

(**b₂**) No-load airgap flux density waveform

(**c₁**) No-load airgap flux density waveform

(**c₂**) No-load airgap flux density waveform

(**d₁**) No-load airgap flux density spectrum

(**d₂**) No-load airgap flux density spectrum

**Figure 6.** *Cont.*

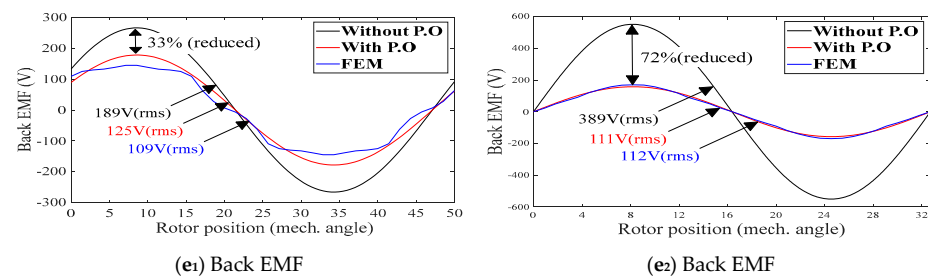(**e₁**) Back EMF         (**e₂**) Back EMF

**Figure 6.** Spoke PM veriner (Subscript 1 and 2 represents the model with 9–slots/7–PM pairs and model with 12–slots/11–PM pairs, respectively).

Then, for each machine the no-load flux lines are shown in Figure 6(b₁,b₂) and the air gap flux density waveforms obtained using the proposed expression (22) in both the manners are compared in Figure 6(c₁,c₂). Figure 6(d₁,d₂), the spectrum of air gap flux density harmonics, which clearly shows the suppression of working modulation flux. From the results of Figure 5, the magnitude of the $Z_{1-}^{mod}$ th modulation flux harmonic is expected to be suppressed about 58% and 89% for $G_1^{low}$ of 3.5, and 11, respectively, from those without considering the potentials oscillation. The FEM results in Figure 6(d₁,d₂) validate the accuracy of the predicted suppression of modulation flux harmonic of order $Z_{1-}^{mod}$, in both models. Furthermore, the modulation fluxes with the harmonic order of $Z_{n+}^{mod}$ such as the 16th in Figure 6(d₁) and the 24th in Figure 6(d₂), though having little contribution to the back-EMF, are oppositely increased by the potentials oscillation as predicted in (22), which proves the accuracy of the proposed equations.

Finally, Figure 6(e₁,e₂) compares the no-load back EMF waveforms from FEM and the analytical calculation using (24), where the analytically obtained ones have no distortion since no time harmonics are included in the calculations. Additionally, the rms values of the fundamental component of back EMF are expressed in Figure 6(e₁,e₂). It can be seen that the calculated back EMFs with potential oscillation is much closer to the FEM results. Indeed, it is because the modulation flux harmonics much reduced and is more serious as the gear ratio is larger as anticipated from the air gap flux density results.

4.2.2. Flux Switching Machine

To verify the effects of potential oscillations on the FSPM machine, two FSPM models of Figure 4c,d are investigated. The one has 12–slots/10–rotor poles ($\gamma_z = 0.833$) with FSC winding, commonly used model in literature [20], with a quite low gear ratio of $G_1^{up} = 2.5$.

Unlike vernier machines, various $Z_{n-}^{mod}$th modulation fluxes contribute to the back EMF. In this regard, $G_3^{up} = 1.25$ for the $Z_{3-}^{mod}$th is not negligible. The other has IS windings, 18-slots/10-rotor poles ($\gamma_z = 0.55$), gear ratio $G_1^{up} = 10$ much larger and $G_3^{up} = 0.58$ smaller than the prior's. As before, the air gap MMF of both models are calculated analytically (their waveform is shown in Appendix B), and their Fourier representation is illustrated in Figure 7(a₁,a₂) which clearly show that the oscillating MMF $F_{1-}^{\Delta}$ of the model with $G_1^{up} = 10$ is much larger than that of one with $G_1^{up} = 2.5$. Also, the $Z_{3-}^{mod}$th MMF $F_{3-}^{\Delta}$ of both models are negligible, so it is expected to not to suppress the modulation flux with $G_3^{up} = 1.25$ and 0.58, respectively.

Next, the no-load flux lines are shown in Figure 7(b₁,b₂), and then the air-gap flux density waveforms are compared with those obtained using (25) in Figure 7(c₁,c₂). The harmonic spectra of the air gap flux density waveforms are shown in Figure 7(d₁,d₂). According to the results for $\gamma_z = 0.833$ and 0.55 in Figure 5, the $Z_{1-}^{mod}$th modulation flux harmonics is suppressed about 15% and 84%, respectively, due to the potential oscillations. Meanwhile, the $Z_{3-}^{mod}$th modulation flux harmonic is predicted to slightly increase for both. The FEM results compared in Figure 7d evidently validate those predictions. It is also notable the $Z_{1+}^{mod}$th modulation fluxes, though their negligible contribution to the back
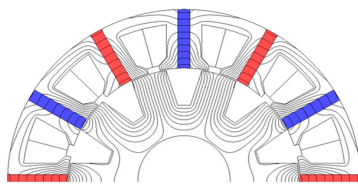
EMF, increase due to the MMF $F_{1+}^{\Delta}$, as can be expected from (25). These results endorse the accuracy of the proposed analytical equations for potential oscillations.
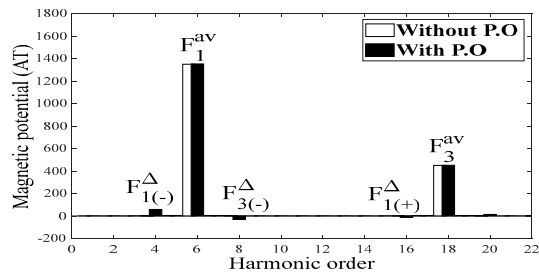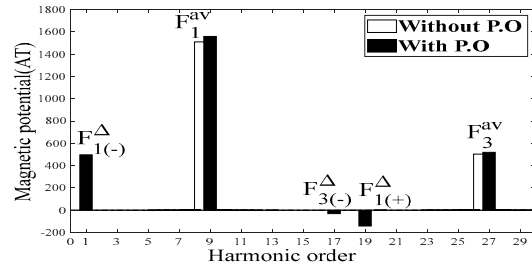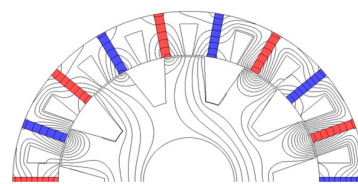


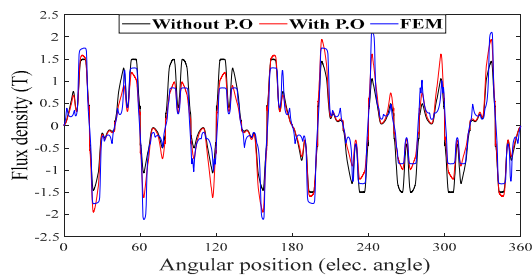(**a₁**) No-load airgap magnetic potential
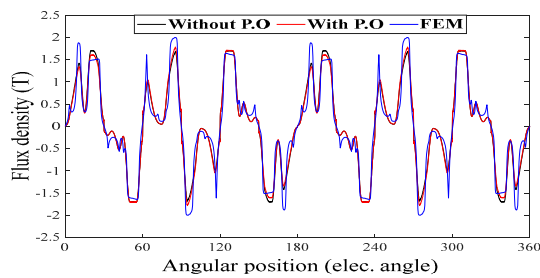


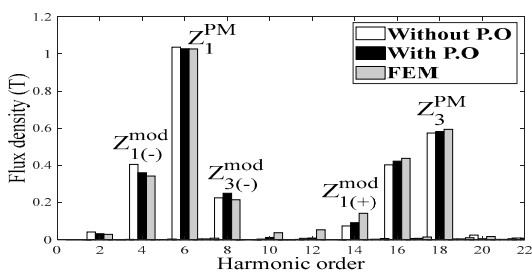(**a₂**) No-load airgap magnetic potential



(**b₁**) No-load airgap flux density waveform



(**b₂**) No-load airgap flux density waveform
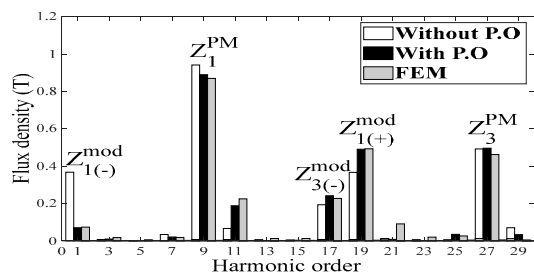


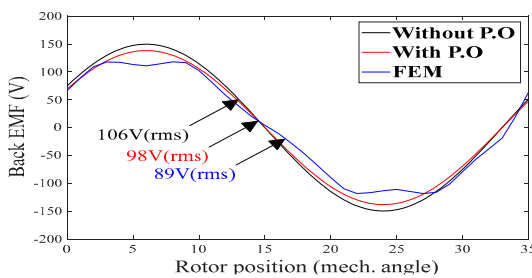(**c₁**) No-load airgap flux density waveform



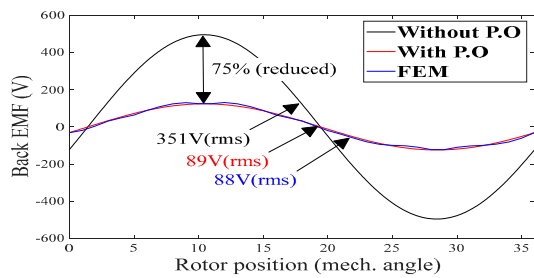(**c₂**) No-load airgap flux density waveform



(**d₁**) No-load airgap flux density spectrum



(**d₂**) No-load airgap flux density spectrum



(**e₁**) Back EMF



(**e₂**) Back EMF

**Figure 7.** FSPM (Subscript 1 and 2 represents the model with 12–slots/10–rotor poles model with 18–slots/10–rotor poles, respectively).

Finally, Figure 7(e$_1$,e$_2$) compares the no-load back EMF waveforms from FEM and the analytical calculation using (26). The rms value of the fundamental component of back EMF is also stated in Figure 7(e$_1$,e$_2$). It is seen that the machine with 12-slots/10 rotor poles ($G_{1,3}^{up}$ = 2.5, 1.25) has insignificant difference in the analytically calculated back EMF values, because the modulation fluxes with moderate gear ratios are little suppressed by the potential oscillations and they produce a back EMF in cooperations.

However, the one with 18-slots/10-rotor poles ($G_{1,3}^{up}$ = 10, 0.55) has a huge difference between the back EMF values, which is evidently due to considerable reduction of the $Z_{1-}^{mod}$th modulation flux and negligible gear ratio of $G_3^{up}$. It is evident that the analytically calculated back EMFs with consideration of oscillations are in very good accordance with the FEM results which validates the proposed method. It is interesting to note that both the FSPM machines with very different $G_1$ finally have almost same back EMF. In this case, of course, the FSC winding would be preferred over the IS winding with a much longer end turn length.

## 5. Conclusions

This study presents an accurate analytical modeling of the scalar magnetic potential oscillation phenomena that uniquely occur in spoke PM flux modulation machines and cause the suppression of modulation fluxes. An air gap MMF equation clearly explaining the phenomena is newly proposed and is further utilized to derive the accurate expression for the air gap flux density and back EMF for each spoke PM machine. By using the derived expressions for each spoke PM machine type, the effects of the potential oscillations on the flux modulation characteristics are quantitatively investigated for various slot-pole combinations. The high accuracy of the calculation results are confirmed by comparing them with the FEM results. After comprehensively investigating the potential magnetic oscillations for each spoke PM machine type, the following conclusions were obtained:

First, in the case of conventional spoke PM machines, the modulation flux has negligible contribution in the back EMF production, thus, the phenomenon of potential oscillations seems irrelevant. The proposed equations clearly show that conventional spoke PM machine with IS winding has zero suppression, however, with FSC winding there exists a certain suppression ratio, but the associated gear ratio is too small to have any significant impact on machine performance. Therefore, it is deduced that the potential oscillations have no effect on the performance of conventional spoke PM machine.

Secondly, the spoke PM vernier machine has considerable suppression of modulation flux due to the potential oscillations. Furthermore, it is revealed that the degree of suppression is interlinked with the machine's slot-pole combination and the resulting gear ratio; however, it is independent with the winding configuration. For instance, for a gear ratio of 5 the suppression ratio is 65% and for a gear ratio of 11 it is as high as 89%, which clearly shows that the suppression increases as the gear ratio gets higher.

Finally, for the flux-switching PM (FSPM) machine, the case is more appealing because there are multiple modulation fluxes with various gear ratios and winding factors, and for each modulation flux there exists a certain suppression ratio. It is revealed that FSPM machine with IS winding, despite having a higher gear ratio, has poor back EMF characteristics, mainly due to a higher suppression ratio of 50% or higher. In contrast, unlike the previous case, FSPM machines with FSC winding have same high winding factor for every working harmonic, in addition, the suppression ratios are relatively low and, more interestingly, it is found that some modulation fluxes have even positive impact due to the potential oscillation phenomenon. Therefore, it is clear that FSPM with FSC winding, despite their lower gear ratios, are more desirable than that of the FSPM with IS winding.

**Author Contributions:** Conceptualization, L.U.R., A.R. and B.K.; methodology, L.U.R. and B.K.; software, L.U.R.; validation, L.U.R.; formal analysis, L.U.R.; investigation, L.U.R.; resources, B.K.; data curation, L.U.R.; writing—original draft preparation, L.U.R.; writing—review and editing, L.U.R., A.R. and B.K.; supervision, B.K.; project administration, B.K.; funding acquisition, B.K. All authors have read and agreed to the published version of the manuscript.

**Data Availability Statement:** Not applicable.

**Conflicts of Interest:** The authors declare no conflict of interest.

## Nomenclature

| | |
|---|---|
| $Z_U$ | Number of slots |
| $Z_L$ | PMs/Number of iron core pieces |
| $Z^{PM}$ | PM Pole pairs |
| $Z^{mod}$ | Modulation pole pair |
| $g$ | Air gap length |
| $r_g$ | Radius of air gap |
| $l_{stk}$ | Stack length |
| $F_{pm}$ | PM magneto magneto-motive force |
| $R_m$ | Magnetic reluctance |
| $R_l$ | Leakage reluctance |
| $\Omega_k$ | Scalar magnetic potential |
| $\Omega_{av}$ | Average/fixed potential value |
| $\Omega_\Delta$ | Oscillating potential value |
| $\Phi_k$ | Air gap flux |
| $\Phi_{m.k}$ | Flux from PM |
| $\Phi_{leak}$ | Leakage flux |
| $P_{g.k}$ | Lumped permeance connected to k$^{th}$ core piece. |
| $P_{av}$ | Average value Lumped permeance |
| $P_1$ | Harmonic permeance |
| $\Lambda_U$ | Permeance function of upper side |
| $\Lambda_L$ | Permeance function of lower side |
| $\lambda$ | Permeance' coefficient |
| $\theta$ | Stationary axis |
| $\theta_m$ | Mover position in the air gap |
| $\theta^r$ | Angle in mover reference |
| $k_w$ | Winding factor |
| $\theta_{span}$ | Mechanical angular span of coil |
| $G^{low}$ | Gear ratio of vernier machine |
| $G^{up}$ | Gear ratio of FSPM machine |
| $\gamma_z$ | Ratio of slots and PMs |
| $\alpha$ | Suppression ratio |
| FSC | Fractional slot oncentrate winding |
| IS | Integral slot winding |
| P. O | Potential oscillation |

## Appendix A

$F_g{}^\Delta$ can be also expressed as Fourier series as

$$\sum\nolimits_{i=1} a_i \cos i\theta^r + b_i \sin i\theta^r \tag{A1}$$

where $i$ = 1, 2, 3, . . .

The coefficient $a_i$ can be obtained as

$$
\begin{aligned}
a_i \quad &= \tfrac{1}{\pi}\int_0^{2\pi} F_g^\Delta \cos i\theta^r d\theta^r = \tfrac{1}{\pi}\sum_{k=1}^{2Z^{PM}} \int_{\theta_k^r}^{\theta_{k+1}^r} F_g^\Delta \cos i\theta^r d\theta^r \\
&= \tfrac{\Omega_{\Delta1}}{\pi}\sum_{k=1}^{2Z^{PM}} \int_{\theta_k^r}^{\theta_{k+1}^r} \cos\big((Z_U - Z^{PM})\theta_k^r + Z_U\theta_m + \gamma_z\pi\big)\cos i\theta^r d\theta^r \\
&= \tfrac{2\Omega_\Delta}{\pi i}\sin\left(\tfrac{\pi i}{2Z^{PM}}\right)X_i
\end{aligned}
$$

where $X_i = \sum_{k=1}^{2Z^{PM}} (-1)^{k-1} \cos(r_z \pi (2k-1) + Z_U \theta_m) \cos\left(\frac{(2k-1)}{2Z^{PM}} i\pi\right)$.

Similarly, $b_i$ can be given as

$$b_i = \frac{2\Omega_\Delta}{\pi i} \sin\left(\frac{\pi i}{2Z^{PM}}\right) Y_i$$

where $Y_i = \sum_{k=1}^{2Z^{PM}} (-1)^{k-1} \cos(r_z \pi (2k-1) + Z_U \theta_m) \sin\left(\frac{(2k-1)}{2Z^{PM}} i\pi\right)$.

$X_i$ and $Y_i$ can be obtained by solving the sum of a geometric sequence through Euler's therom, and they have non-zero values of (A2) and (A3) when $i = nZ^{PM} \pm Z_U$ (where $n$ is a positive odd integer).

$$X_{nZ^{PM}\pm Z_U} = Z^{PM}(-1)^{\frac{n+1}{2}} \sin Z_U \theta_m \tag{A2}$$

$$Y_{nZ^{PM}\pm Z_U} = -Z^{PM}(-1)^{\frac{n+1}{2}} \cos Z_U \theta_m \tag{A3}$$

By using (A2) and (A3) and replacing $i$ in (A1) with $nZ^{PM} \pm Z_U$, $F_g^\Delta$ can obtained as

$$F_g^\Delta = \frac{\Omega_\Delta}{\pi} \cos \gamma_Z \pi \sum_{n=odd} \pm \frac{2 \sin\left(Z_U \theta_m + (Z_U \pm nZ^{PM})\theta^r\right)}{n \pm 2\gamma_z}$$

Finally, replacing $\theta^r$ with $\theta - \theta_m$, equation (19) can be obtained.

**Appendix B**

Illustration of oscillation phenomena of scalar magnetic potential of rotor and stator core pieces of spoke PM vernier and FSPM machine, respectively. The Fourier representation of these waveform is shown in Section 4.
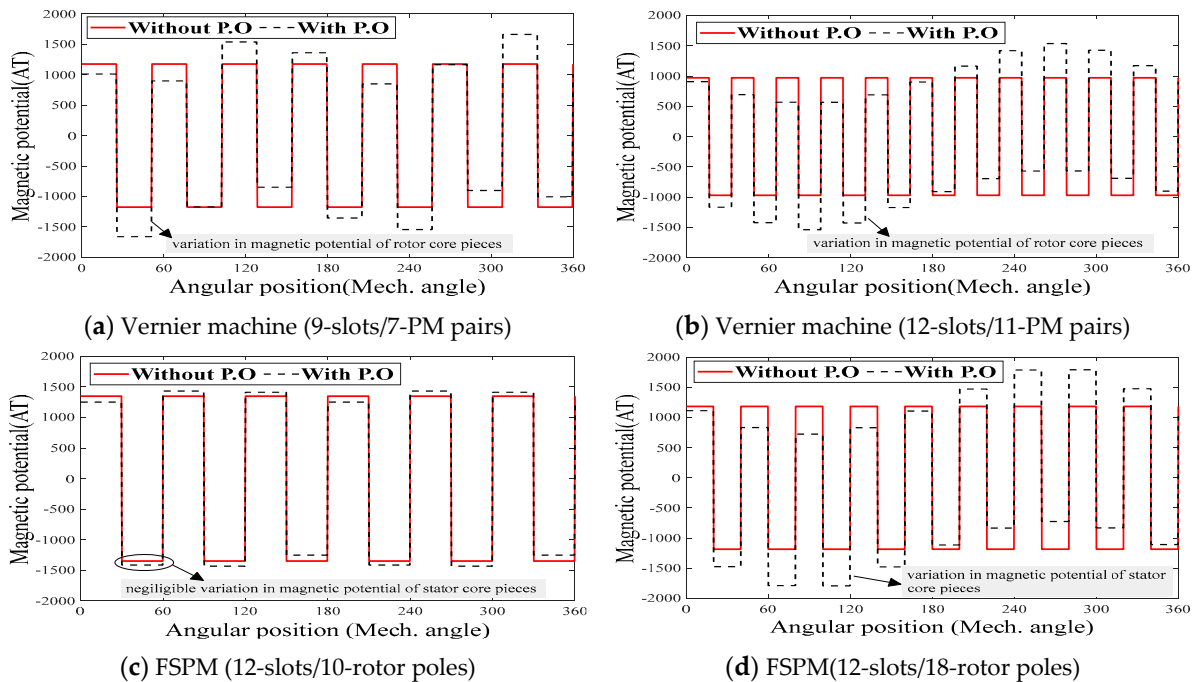


**(a)** Vernier machine (9-slots/7-PM pairs)

**(b)** Vernier machine (12-slots/11-PM pairs)

**(c)** FSPM (12-slots/10-rotor poles)

**(d)** FSPM(12-slots/18-rotor poles)

**Figure A1.** Illustration of scalar magnetic potential oscillation of core pieces.

# References

1.  Vukotić, M.; Miljavec, D. Design of a Permanent-magnet Flux-modulated Machine with a High Torque Density and High Power Factor. *IET Electr. Power Appl.* **2016**, *10*, 36–44. [CrossRef]
2.  Liu, C. Emerging Electric Machines and Drives—An Overview. *IEEE Trans. Energy Convers.* **2018**, *33*, 2270–2280. [CrossRef]
3.  Ur Rahman, L.; Khan, F.; Khan, M.A.; Ahmad, N.; Khan, H.A.; Shahzad, M.; Ali, S.; Ali, H. Modular Rotor Single Phase Field Excited Flux Switching Machine with Non-Overlapped Windings. *Energies* **2019**, *12*, 1576. [CrossRef]
4.  Niu, S.; Ho, S.L.; Fu, W.N.; Wang, L.L. Quantitative Comparison of Novel Vernier Permanent Magnet Machines. *IEEE Trans. Magn.* **2010**, *46*, 2032–2035. [CrossRef]
5.  Li, J.; Chau, K.T.; Jiang, J.Z.; Liu, C.; Li, W. A New Efficient Permanent-Magnet Vernier Machine for Wind Power Generation. *IEEE Trans. Magn.* **2010**, *46*, 1475–1478. [CrossRef]
6.  Zhu, X.; Lee, C.H.T.; Chan, C.C.; Xu, L.; Zhao, W. Overview of Flux-Modulation Machines Based on Flux-Modulation Principle: Topology, Theory, and Development Prospects. *IEEE Trans. Transp. Electrif.* **2020**, *6*, 612–624. [CrossRef]
7.  Kim, B. Design Method of a Direct-Drive Permanent Magnet Vernier Generator for a Wind Turbine System. *IEEE Trans. Ind. Appl.* **2019**, *55*, 4665–4675. [CrossRef]
8.  Rehman, A.; Kim, B. Characteristics Analysis of Consequent-Pole Ferrite Magnet Vernier Machine Using Novel Equivalent Magnetic Circuit. *IEEE J. Emerg. Sel. Top. Power Electron.* **2022**, *10*, 1823–1833. [CrossRef]
9.  Chen, Q.; Liu, G.; Zhao, W.; Shao, M. Nonlinear Adaptive Lumped Parameter Magnetic Circuit Analysis for Spoke-Type Fault-Tolerant Permanent-Magnet Motors. *IEEE Trans. Magn.* **2013**, *49*, 5150–5157. [CrossRef]
10. Carraro, E.; Bianchi, N.; Zhang, S.; Koch, M. Design and Performance Comparison of Fractional Slot Concentrated Winding Spoke Type Synchronous Motors with Different Slot-Pole Combinations. *IEEE Trans. Ind. Appl.* **2018**, *54*, 2276–2284. [CrossRef]
11. Azeem, M.; Kim, B. Electromagnetic Analysis and Performance Investigation of a Flux-Switching Permanent Magnet Machine. *Energies* **2019**, *12*, 3362. [CrossRef]
12. Li, D.; Qu, R.; Li, J.; Xu, W.; Wu, L. Synthesis of Flux Switching Permanent Magnet Machines. *IEEE Trans. Energy Convers.* **2016**, *31*, 106–117. [CrossRef]
13. Kim, B.; Lipo, T.A. Operation and Design Principles of a PM Vernier Motor. *IEEE Trans. Ind. Appl.* **2014**, *50*, 3656–3663. [CrossRef]
14. Kim, B.; Lipo, T.A. Analysis of a PM Vernier Motor with Spoke Structure. *IEEE Trans. Ind. Appl.* **2016**, *52*, 217–225. [CrossRef]
15. Zou, T.; Li, D.; Qu, R.; Jiang, D. Performance Comparison of Surface and Spoke-Type Flux-Modulation Machines with Different Pole Ratios. *IEEE Trans. Magn.* **2017**, *53*, 1–5. [CrossRef]
16. Ren, X.; Li, D.; Qu, R.; Yu, Z.; Gao, Y. Investigation of Spoke Array Permanent Magnet Vernier Machine with Alternate Flux Bridges. *IEEE Trans. Energy Convers.* **2018**, *33*, 2112–2121. [CrossRef]
17. Zhu, Z.Q.; Howe, D. Instantaneous Magnetic Field Distribution in Brushless Permanent Magnet DC Motors. III. Effect of Stator Slotting. *IEEE Trans. Magn.* **1993**, *29*, 143–151. [CrossRef]
18. Kim, B. Investigation on Slot–Pole Combinations of a PM Vernier Motor with Fractional-Slot Concentrated Winding Configurations. *Energies* **2017**, *10*, 1310. [CrossRef]
19. Tlali, P.M.; Wang, R.-J.; Gerber, S.; Botha, C.D.; Kamper, M.J. Design and Performance Comparison of Vernier and Conventional PM Synchronous Wind Generators. *IEEE Trans. Ind. Appl.* **2020**, *56*, 2570–2579. [CrossRef]
20. Chen, J.T.; Zhu, Z.Q. Winding Configurations and Optimal Stator and Rotor Pole Combination of Flux-Switching PM Brushless AC Machines. *IEEE Trans. Energy Convers.* **2010**, *25*, 293–302. [CrossRef]